This project has received funding from the European Union's Seventh Programme for research, technological development and demonstration under grant agreement No [308417]".

# New Directions in Seismic Hazard Assessment through Focused Earth Observation in the Marmara Supersite

Grant Agreement Number: 308417
co-funded by the European Commission within the Seventh Framework Programme
THEME [ENV.2012.6.4-2]
[Long-term monitoring experiment in geologically active regions of Europe prone to natural hazards: the Supersite concept]

# D3.2

# Deformation map obtained by applying the SBAS and/or PSI technique to a sample C-band SAR data set

| | |
|---|---|
| Project Start Date | 1 November 2012 |
| Project Duration | 42 months |
| Project Coordinator /Organization | Nurcan Meral Özel / KOERI |
| Work Package Number | WP3 |
| Deliverable Name/ Number | 3.2 |
| Due Date Of Deliverable | 30 April 2016 |
| Actual Submission Date | 15 May 2016 |
| Organization/Author (s) | BRGM/de Michele M., KOERİ/Ergintav S. |

| **Dissemination Level** | | |
|---|---|---|
| PU | Public | |
| PP | Restricted to other programme participants (including the Commission) | |
| RE | Restricted to a group specified by the consortium (including the Commission) | |
| CO | Confidential, only for members of the consortium (including the Commission) | |

## TABLE OF CONTENTS

# 1. Context

## 1.1 Marsite project

"The 1999 disastrous İzmit earthquake (Mw=7.4) was not a surprise because westward migrating earthquakes that broke ~1000 km-long section of North Anatolian Fault (NAF) in a manner of falling dominos had already arrived nearby İzmit. Another large and destructive earthquake is now expected to occur further west along the North Anatolian fault under the Sea of Marmara, 20 km south of Istanbul, one of the most populous and rapidly growing cities of Europe. Historical documents going back to two millennia indicate that many destructive earthquakes stroke the city of Istanbul since the northern segment of the NAF under the Marmara Sea accommodates most of the plate motion between Anatolia and Eurasia. The probability of a large earthquake to strike Istanbul again is estimated to be about 65% over the next 30 years." [from Marsite Project Introduction].

The present deliverable aims at showing the results retrieved from C band Interferometric Synthetic Aperture Radar (InSAR) measurements for the monitoring of Crustal Deformation in the Anatolian Fault Zone in the frame of the MARMARA SUPERSITE PROJECT "MARSITE".

We proposed to process SAR data made available through the CAT-1 ESA (European Space Agency) archives, acquired by the C-band radar sensor Envisat ASAR, to retrieve surface displacements map on selected areas of the Anatolian Fault Zone (AFZ). In principle this exercise would allow us to test if C band SAR signal coherence is high enough to allow us to map the spatial and temporal evolution of the present-day crustal deformation phenomena affecting the MARsite Area with high level of spatial details. The goal of this task is to assess whether InSAR C-Band data can be useful to evaluate the long-term behavior of the Ganos section of the NAFZ, complementarily to GPS measurements and other in-situ observations. Besides, since InSAR maps motions of all nature occurring at the ground surface, we might expect to observe not only tectonic phenomena but also local subsidence due to land-sliding or sediment compaction.

In this specific task, mid-term monitoring (4 - 10 years) of the crustal deformation in the MARsite area is investigated by using InSAR stacking approach. During the MARsite project

kick off meeting in Istanbul (2012), the WP3 group decided to select a specific section of the North Anatolian Fault Zone (NAFZ) to be used as a laboratory for C-band and C-band InSAR; the selected one is the Ganos section of the NAFZ, where our study is therefore concentrated.

Here in this deliverable, we aim at providing the C-band data acquisition frame, the data processing strategy, the results. A preliminary analysis of the results and some hints for further investigations are also highlighted. In a second step, we might aim at post-processing the results of this task and use them, if relevant, for characterizing the faults behavior.

# 2 C-band InSAR on the Ganos section of the NAFZ

## 2.1 Tectonic context of the study area

The North Anatolian Fault (NAF), with a total length of about 1500 km, is one of the most active right-lateral strike–slip faults in the world. It defines the tectonic boundary between the Anatolian Plate and the Eurasian Plate in northern Turkey, accommodating ~14–30 mm/yr of relative plate motion between the two plates (fig. 1). The Gazikoy–Saros segment (the Ganos fault, GF) is the onshore segment of the northern strand of the NAF between the Marmara Sea and the Gulf of Saros. It was last ruptured in 1912 with a Ms=7.4 earthquake that broke the entire inland segment of the fault, a length of about 50 km, and produced a right-lateral strike–slip component of at least 3 m. Other large historical earthquakes that have been attributed to the Ganos fault occurred in A.D. 824, 1343, 1509 and 1766 (e. g. Reilinger et al., 2000; Meade et al., 2002; Motagh et al., 2007; Janssen et al., 2009; Megraoui et al., 2012 ; Ersen Aksoy et al., 2010).

The GF forms a 45 km long linear fault system and represents the link between the northern strand of the NAFZ in the Sea of Marmara and the North Aegean Trough where slip partitioning results in branching of the fault zone (e.g. Barka and Kadin sky- Cade,1988; Okay et al.,1999).

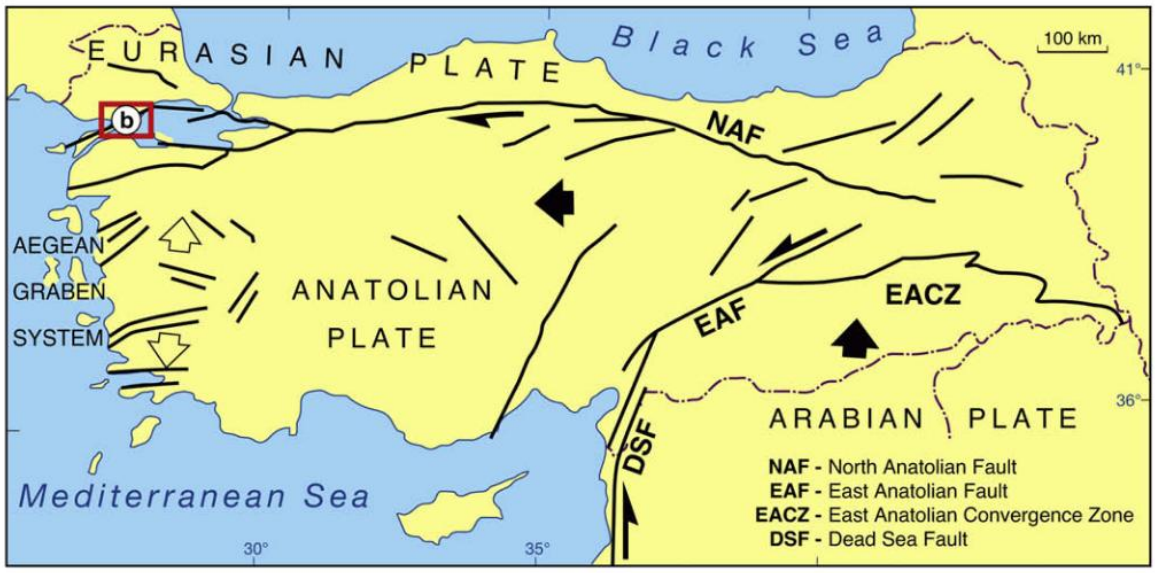


**Figure 1. The NAFZ. The red rectangle represents the Envisat study area centered on the Ganos fault (after Janssen et al., 2009).**

The GF consists of several sub-parallel faults, which are separated by less than 1 km (Okay et al., 2004). The trace of the fault is clearly discernable on the SRTM DEM image with its northeastern part being bounded by the Ganos Mountains. A dominant right-lateral strike-slip motion became active toward the end of the Miocene and formed the Ganos Mountains due to transpressional uplift (Okay et al., 1999). Since the latest Miocene the total accumulated right-lateral displacement is in the order of 40 km (Okay et al., 1999). At present, the GF accommodates fault-normal convergence at a rate of 1.1 ±0.4 mm/yr (fig. 2a, b) (Okay et al., 2004; Ergintav et al., 2012; 2014). Tuysuz et al. (1998) interpreted the apparent lack of seismicity for magnitudes larger than 3 along the GF as an indication for a locked fault segment that slips only during large earthquakes. Recent interferometry and GPS measurements estimated a fault locking depth in the range of 8-17 km (Motagh et al., 2007, Ergintav et al., 2012; 2014).

Seismicity in the western Marmara Sea region predominantly occurs offshore along the main branch of the NAFZ (Bogazii University Kandilli Observatory and Earthquake Research Institute/KOERI, earthquake catalogue for 1900-2005; Ergintav et al., 2012). The GF is almost aseismic down to Mc  2.7 magnitude threshold and a diffuse distribution of hypocenters is observed offshore. In particular, seismicity clusters occur NW of Marmara Island and in the Tekirdag Basin (fig. 3). The three largest earthquakes in the GF region during the last century

occurred in 1912 within only a few days. Two events occurred along the GF with surface wave magnitudes (Ms) of 7.3 and Ms 6.2, respectively. The rupture of the 1912 mainshock extended along the entire onshore segment between Marmara Sea and Gulf of Saros.

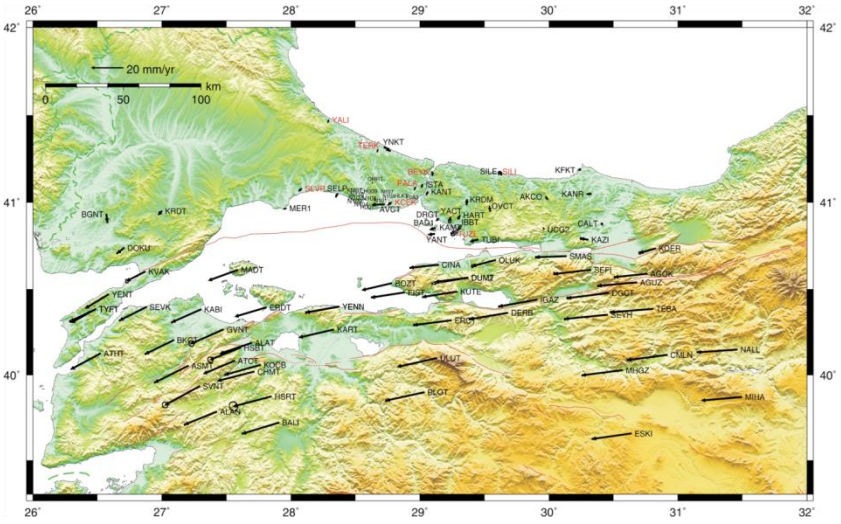


Figure 2a. GPS velocities on the MARsite area (after Ergintav et al., 2012)

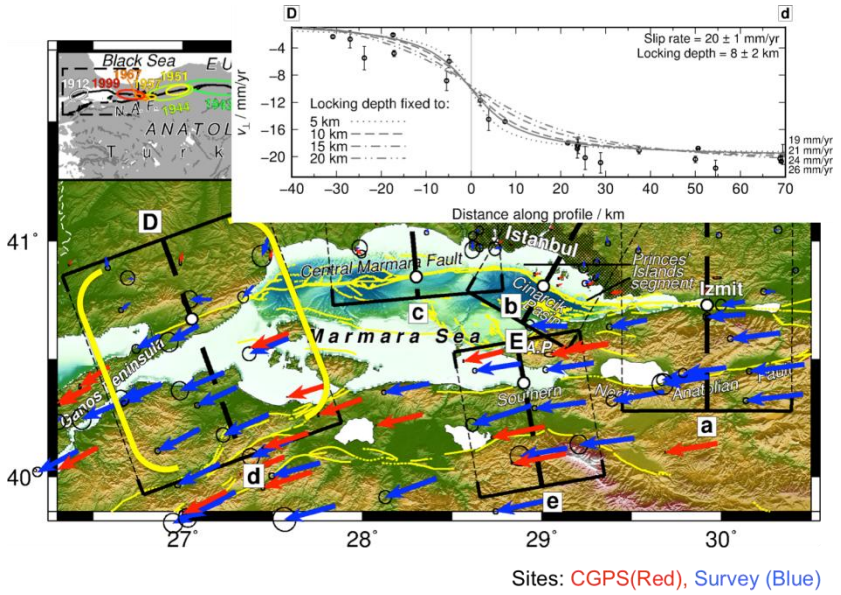


Figure 2b. GPS profiles on the Ganos section of the NAFZ (after Ergintav et al., 2014).

Based on sea floor observations, Armijo et al. (2005) suggested that the rupture even extended into the Marmara Sea. The last earthquake at the GF (M> 4) occurred in 1985 in

the Ganos Mountains with a reverse faulting mechanism on a NE striking fault plane (Janssen et al., 2009).

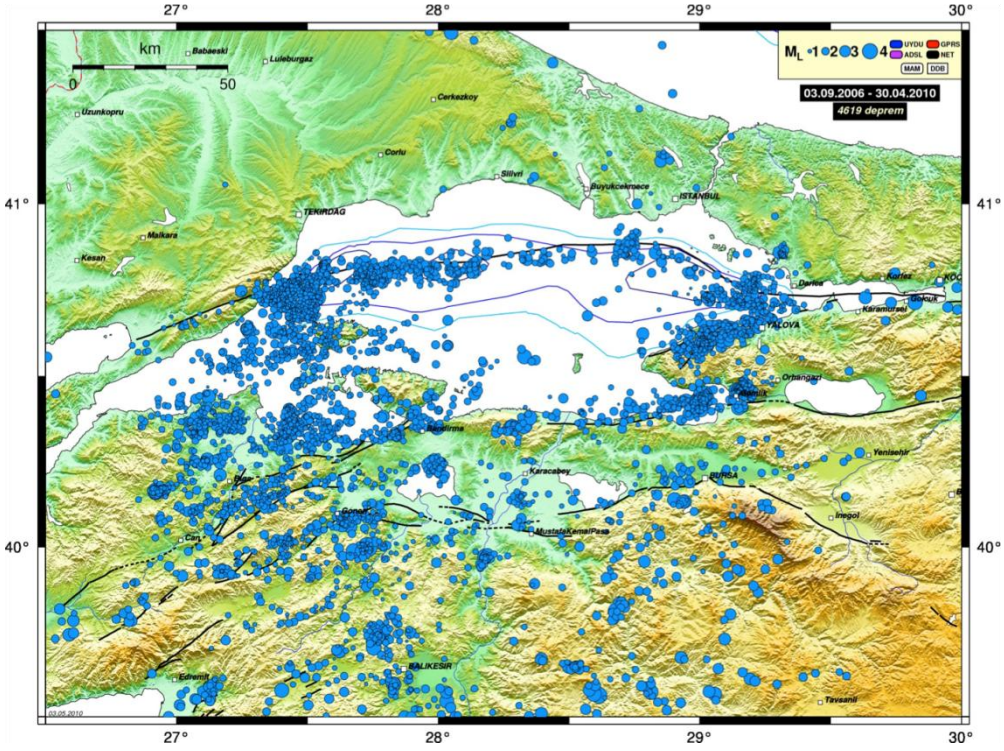


Figure 3. Seismicity of the MARsite area -2006/2010- (after Ergintav et al., 2012).

## 2.2 C-BAND INSAR

### 2.2.1 Data acquisition and processing

The Envisat archive over the Ganos Section of the NAFZ is not extraordinarily rich concerning the number of SAR scenes acquired with the same viewing and polarization mode, which is a necessity when willing to perform a standard InSAR study. We then processed 26 Single Look Complex (SLC), IS2 mode, C-band data spanning 8 years, from 2002 to 2010 (tab 1).

ENVISAT InSAR can map ground deformation at a spatial resolution of tens of meters with sub centimeter precision in the line-of-sight direction (LOS) of the satellite (e.g., Massonnet and Feigl, 1998). We acquired all available ENVISAT archived data for the Ganos section of the NAFZ. We chose to process the ascending orbit ENVISAT acquisitions as the satellite path

orientation with respect to the fault orientation is optimal to obtain a suitable InSAR LOS sensitivity to strike-slip surface movement parallel to the NAFZ at the Ganos section. The shallow creep signal is expected to range from ~0 to 1.5 cm/yr. Atmospheric delays in the radar images of the interferometric pair could mask this kind of signal in a single interferogram (Puysségur et al., 2007; Zebker et al., 1997).

| date | sensor | mode | look angle |
|---|---|---|---|
| *21/11/2002* | *ASAR* | *IS2* | *21°* |
| *06/03/2003* | *ASAR* | *IS2* | *21°* |
| *28/08/2003* | *ASAR* | *IS2* | *21°* |
| *06/11/2003* | *ASAR* | *IS2* | *21°* |
| *15/01/2004* | *ASAR* | *IS2* | *21°* |
| *25/03/2004* | *ASAR* | *IS2* | *21°* |
| *29/04/2004* | *ASAR* | *IS2* | *21°* |
| *03/06/2004* | *ASAR* | *IS2* | *21°* |
| *08/07/2004* | *ASAR* | *IS2* | *21°* |
| *12/08/2004* | *ASAR* | *IS2* | *21°* |
| *21/10/2004* | *ASAR* | *IS2* | *21°* |
| *30/12/2004* | *ASAR* | *IS2* | *21°* |
| *03/02/2005* | *ASAR* | *IS2* | *21°* |
| *28/07/2005* | *ASAR* | *IS2* | *21°* |
| *10/11/2005* | *ASAR* | *IS2* | *21°* |
| *30/03/2006* | *ASAR* | *IS2* | *21°* |
| *13/07/2006* | *ASAR* | *IS2* | *21°* |
| *08/02/2007* | *ASAR* | *IS2* | *21°* |
| *06/09/2007* | *ASAR* | *IS2* | *21°* |
| *15/11/2007* | *ASAR* | *IS2* | *21°* |
| *10/09/2009* | *ASAR* | *IS2* | *21°* |
| *15/10/2009* | *ASAR* | *IS2* | *21°* |
| *19/11/2009* | *ASAR* | *IS2* | *21°* |
| *24/12/2009* | *ASAR* | *IS2* | *21°* |
| *28/01/2010* | *ASAR* | *IS2* | *21°* |
| *17/06/2010* | *ASAR* | *IS2* | *21°* |
| *22/07/2010* | *ASAR* | *IS2* | *21°* |

**Table 1 . List of ASAR data used in the present task**

To reduce atmospheric influence on the interferometric phase, we used a stacking methodology. We used the stacking method as implemented in the GAMMA software (Wegmüller et al., 2009; de Michele et al., 2011). The starting point was a set of 27 SLCs

ENVISAT images that were combined to calculate 108 differential interferograms with a perpendicular baseline of less than 500 m. Topographic contributions to the interferometric phase were calculated for each interferogram using the Shuttle Radar Topography Mission (SRTM) 90-m digital elevation model (DEM) (fig. 4) and subtracted from the interferograms. The SRTM DEM was also used in a later stage to project the results into a geographic orthoprojection. From the 108 initial differential interferograms, only a subset of 9 high-signal-coherence interferograms were selected based on visual analysis. Unfortunately, C band signal is not very coherent in the study area, mainly due to vegetation cover changes (fig 5) We chose to stack interferograms with a signal coherence ≥~0.6 on at least ~65% of the dataset. We used the GAMMA Minimum Cost Flow (MCF) algorithm (Costantini and Rosen, 1999; Werner et al., 2002) to unwrap the selected interferograms. For each interferogram, the unwrapping step, performed at the full resolution grid, was improved using a phase reference model obtained by unwrapping the corresponding multiple-look interferogram.

| date (master) | date (slave) | time span (days) |
|---|---|---|
| 03/04/2008 | 17/07/2008 | 105 |
| 15/11/2007 | 03/04/2008 | 140 |
| 25/03/2004 | 03/06/2004 | 70 |
| 25/03/2004 | 29/04/2004 | 35 |
| 28/08/2003 | 06/11/2003 | 70 |
| 06/03/2003 | 06/11/2003 | 245 |
| 21/11/2002 | 28/08/2003 | 280 |
| 21/11/2002 | 25/03/2004 | 490 |
| 21/11/2002 | 06/03/2003 | 105 |

**Table 2. List of selected interferograms (and respective temporal baseline) used in the stacking procedure.**

The phase reference model was then resized to the original pixel resolution (at the full resolution grid).

For each pixel, the unwrapped phase value was computed from the complex valued interferogram under the assumption that the phase values in the resized model correspond to the correct unwrapped phase within the interval $\pm\pi$. The resulting unwrapped phase meets the condition that rewrapping of the unwrapped phase results in exactly the phase of

the complex interferogram, except for a constant offset which can be defined through the phase indicated for the reference location (Werner et al., 2002).

The atmospheric phase delay was also estimated. We observe that, depending on atmospheric conditions, the path delay might have an altitude dependence caused by changes in the atmospheric water vapor and pressure profiles between the acquisitions of the interferometric image pairs (e.g., Doin et al., 2009). In the study region, the atmospheric phase delay is not as exacerbated by extraordinary relief as has been reported elsewhere (e.g., Elliot et al., 2008). To find subtle signals due to land displacements, we used GAMMA to determine the linear regression coefficients of the residual phase with respect to height in the unwrapped interferograms. We used the DEM (in radar geometry) to generate the phase model of the height-dependent atmospheric phase delay for each unwrapped interferogram. Each phase model was then subtracted from the corresponding single unwrapped interferogram.

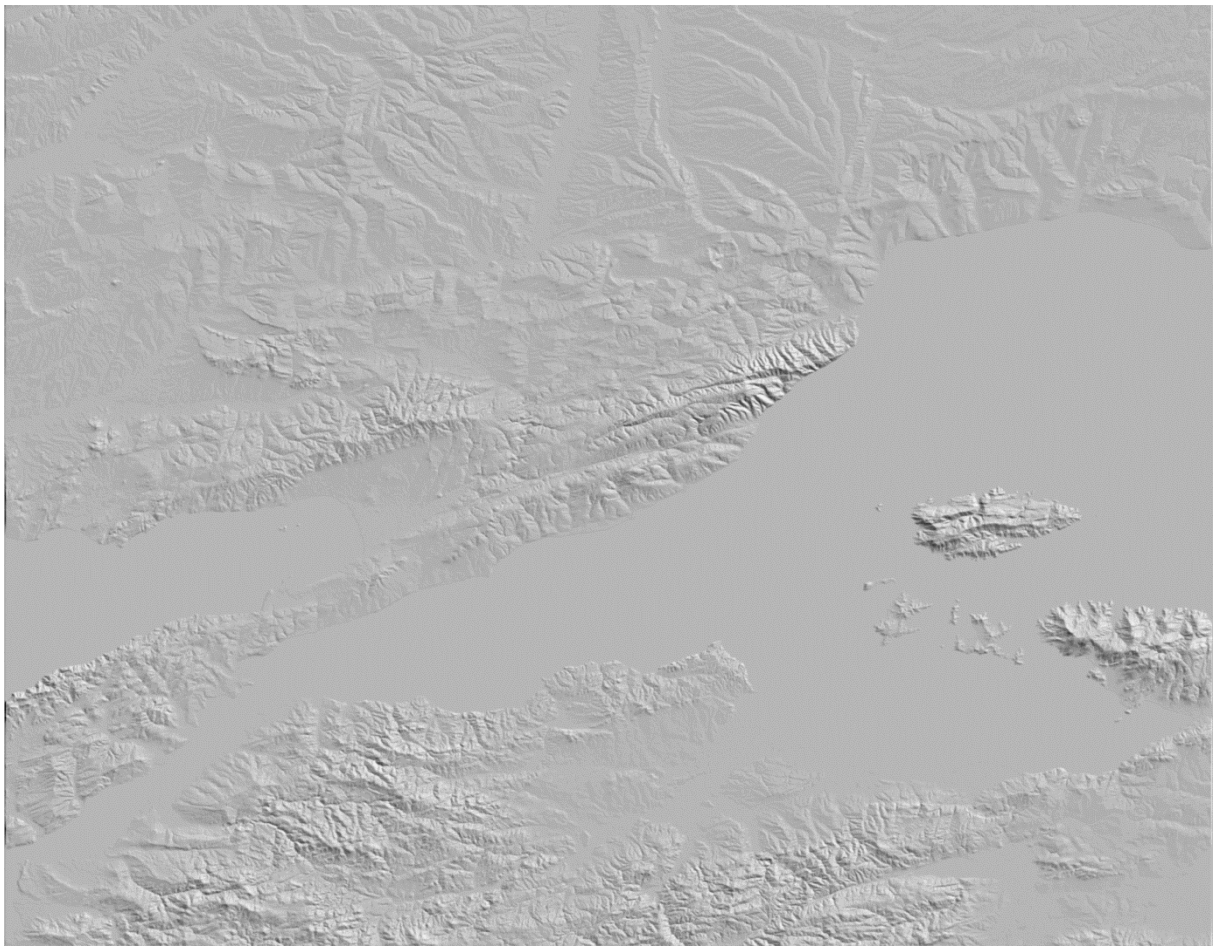

**Figure 4. The shaded DEM from the Shuttle Radar Topography Mission.**

Then, the stacking algorithm was used to estimate the linear rate of differential phase using the set of unwrapped differential interferograms, to derive a time averaged linear velocity map over the study area. The stacking algorithm uses the individual interferogram phases weighted by the time interval in estimating the phase rate. The underlying assumption is that atmospheric statistics are stationary for the set of interferograms while land displacement is not. No a priori models of surface displacement were used in any of the processing steps described above.

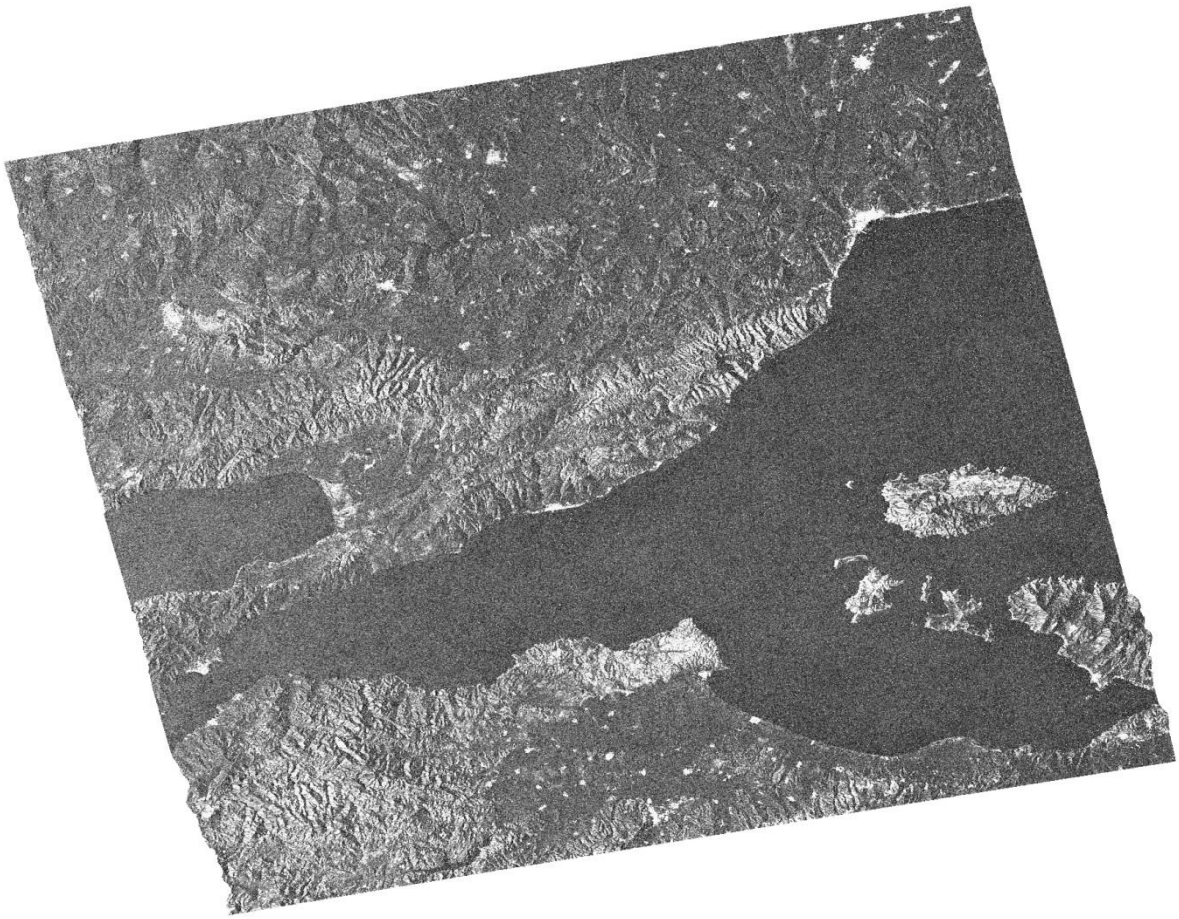

**Figure 5. The average signal coherence map. Black = no coherence ; white = good coherence.**

### 2.2.2 Results

One result of this analysis is the SAR phase linear evolution with time calculated from 2002 to 2010 and measured in the LOS direction of the sensor (fig. 6).

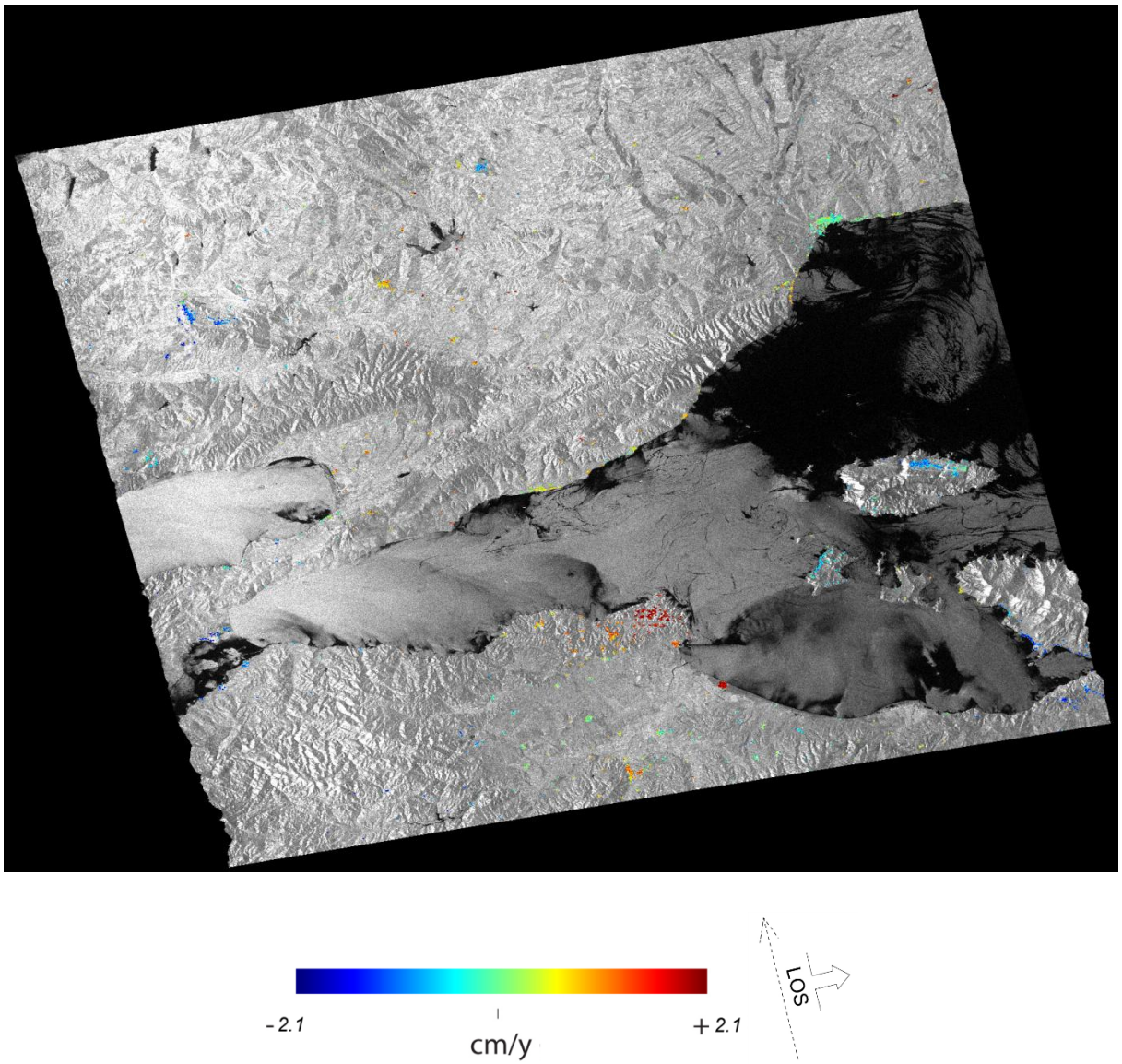


**Figure 6. Results (cm / year ) of the stacking procedure applied on 45 unwrapped interferograms.**

From figure 6, we ca observe that there are few coherent pixels in the final results. The distribution of the coherent pixels and their density are not sufficient to attempt a consistent tectonic interpretation. The velocity values highlighted in figure 6 might be due to shallow, local, phenomena (landsliding? sediment compaction? local subsidence?).

At the present stage, given the low signal coherence, we cannot use these results to make a quantitative interpretation about tectonic motions in the study area. Further processing, maybe using the ESA Sentinel-1, which improved revisit time might improve signal coherence, has to be tested in the area in order highlight the hidden tectonic signal. As far as

our experience is concerned, given the land use in the study area, L-band has to be preferred (ALOS PALSAR 2).

### 2.2.3 Discussion and recommendation

The tectonic signal affecting the Ganos section of the NAFZ cannot be retrieved from the Envisat InSAR velocity map presented in this report. The main reason is that InSAR signal coherence is very low in the study area so that just few coherent pixels could be analyzed in the stacking procedure. Given the scares temporal and spatial data sampling, unfortunately these results are not adapted to the purpose of tectonic studies. Whereas, local subsidence sand landsliding can be highlighted in the velocity map.

In any case, we have to take into considerations that the amount of coherent C-band InSAR data was not extraordinary. 9 interferograms spanning more than 8 years are not so numerous to measure tectonic strain with high level of confidence, considering that the expected tectonic motion, as seen by GPS, is between 0 and 2 cm/year (Ergintav et al., 2014).

Further processing should be foreseen, using the ESA Sentinel-1, which improved revisit time might help in obtaining more coherent InSAR signals in the study area. As far as our experience is concerned, for the measurements of tectonic motions in the study area we recommend L- band InSAR. These data can be provided by the ALOS PALSAR-2 sensor complementary with C-band InSAR provided by the ESA Sentinels.

## Bibliography


Aksoy, M.E., Meghraoui, M., Vallee, M., and Cakir, Z., 2010, Rupture characteristics of the A.D. 1912 Murefte (Ganos) earthquake segment of the North Anatolian fault (Western Turkey): Geology, 38, 991-994.

Armijo R., B. Meyer, A. Hubert, A. Barka, Westward propagation of the North Anatolian fault into the northern Aegean: timing and kinematics, Geology, 1999, 27, 267–270.

Armijo R., N. Pondard, B. Meyer, B. Mercier de Lepinay, G. Ucarkus, J. Malavieille, S. Dominguez, M.-A. Gustcher, Beck, N. Çagatay, Z. Cakir, C. Imren, E. Kadir, Natalin, Marmarascarps Cruise party, Submarine fault scarps in the Sea of Marmara pull-apart (North Anatolian Fault): implications for seismic hazard in Istanbul, 2005, Geochemistry Geophysics Geosystems, 6, doi: 10.1029/2004GC000896

Barka A.A., K. Kadinsky-Cade Strike-slip fault geometry in turkey and its influence on earthquake activity, 1988, Tectonics, 7, 663–684.

Berardino P., G. Fornaro, R. Lanari, E. Sansosti, A new algorithm for surface deformation monitoring based on small baseline differential SAR interferograms, IEEE Trans. Geosci. Remote Sens., 2002, 40, 2375–2383.

Costantini M., P.A. Rosen, A generalized phase unwrapping approach for sparse data, Proceedings, IGARSS '99, Hamburg, Germany (1999), pp. 267–269 June 28–July 2.

de Michele M., D. Raucoules, F. Rolandone, P. Briole, J. Salichon, A. Lemoine, H. Aochi, Spatiotemporal evolution of surface creep in the Parkfield region of the San Andreas Fault (1993–2004) from synthetic aperture radar, Earth and Planetary Science Letters, 2011, 308, 1–2, , 141-150, doi: 10.1016/j.epsl.2011.05.049.

Doin M.-P., C. Lasserre, G. Peltzer, O. Cavalié, C. Doubre, Corrections of stratified tropospheric delays in SAR interferometry: validation with global atmospheric models, 2009, J. Appl. Geophys., 69 (1), 35–50.

Elliot J.R., J. Biggs, B. Parsons, T.J. Wright, InSAR slip rate determination on the Altyn Tagh Fault, northern Tibet, in the presence of topographically correlated atmospheric delays, 2008, Geophys. Res. Lett., 35, L12309 doi: 10.1029/2008GL033659.

Ergintav, S., R. E. Reilinger, R. Çakmak, M. Floyd, Z. Çakır, U. Doğan, R. W. King, S. McClusky, and H. Özener (2014), Istanbul's earthquake hot spots: Geodetic constraints on strain accumulation along faults in the Marmara seismic gap, Geophys. Res. Lett., 41, doi:10.1002/2014GL060985.

Ergintav S., Cakir Z., Dogan U., Cakmak R., Floyd M., King R. W., McClusky S., Reilinger R., Seismic Potential of the North Anatolian Fault in the Sea of Marmara, Turkey, AGU Meeting, December 2014, San Fransisco, USA.

Janssen C., M. Bohnhoff, Y. Vapnik, E. Görgün, F. Bulut, B. Plessen, D. Pohl, M. Aktar, A.I. Okay, G. Dresen, 2009, Tectonic evolution of the Ganos segment of the North Anatolian Fault (NW Turkey), Journal of Structural Geology, 31, 1, 11-28, ISSN 0191-8141, doi:10.1016/j.jsg.2008.09.010.

Massonnet D., K.L. Feigl Radar interferometry and its application to changes in the earth's surface, Rev. Geophys., 1998, 36, 441–500.

Meade B.J., B.H. Hager, S.C. McClusky, R.E. Reilinger, S. Ergintav, O. Lenk, A. Barka, H. Özener, 2002, Estimates of Seismic Potential in the Marmara Sea Region from Block Models of Secular Deformation Constrained by Global Positioning System Measurements, Bull. Seismol. Soc. Am. 92 , 208–215.

Motagh M., J. Hoffmann, B. Kampes, M. Baes, J. Zschau, 2007, Strain accumulation across the Gazikoy–Saros segment of the North Anatolian Fault inferred from Persistent Scatterer Interferometry and GPS measurements, Earth and Planetary Science Letters, 255, 3–4, 432-444, ISSN 0012-821X, doi:10.1016/j.epsl.2007.01.003.

Okay A., E. Demirbag, H. Kurt, N. Okay, I. Kuscu, An active, deep marine strike-slip basin along the North Anatolian Fault in Turkey, 1999, Tectonics, 18, 129–147.

Puysségur B., R. Michel, J.-P. Avouac, Tropospheric phase delay in interferometric synthetic aperture radar estimated from meteorological model and multispectral imagery, J. Geophys. Res., 2007, 112, B05419 doi: 10.1029/2006JB004352.

Reilinger R.E., S. Ergintav, R. Bürgmann, S. McClusky, O. Lenk, A. Barka, O. Gurkan, L. Hearn, K.L. Feigl, R. Cakmak, B. Aktug, H. Ozener, M.N. Töksoz, Coseismic and postseismic fault

slip for the 17 August 1999, M=7.5, Izmit, Turkey Earthquake, 2002, Science, 289, 1519–1524.

Tüysüz O., A. Barka, E. Yigitbas, Geology of the Saros graben and its implications for the evolution of the North Anatolian fault in the Ganos-Saros region, Tectonophysics, 1998, 293, 105–126.

Wegmüller U., C.L. Werner, M. Santoro, Motion monitoring for Etna using ENVISAT time series, Proceedings, ALOS PI Symposium 2009, November 9–13, Hawaii.

Werner C., U. Wegmüller, T. Strozzi, Processing strategies for phase unwrapping for InSAR applications, Proceedings, EUSAR Conference, June 4–6, Cologne, Germany, unpaginated CD-ROM (2002).

Zebker H.A., P.A. Rosen, H. Hansley, Atmospheric effects in interferometric synthetic aperture radar surface deformation and topographic maps, J. Geophys. Res., 1997, 102, 7547–7563.